数理解析研究所講究録
第2076巻 2018年 129-136

傾斜した棒から励起される内部重力波

神戸大学 (Kobe University) 片岡 武 (Kataoka, T.)
Massachusetts Institute of Technology S. J. Ghaemsaidi,
N. Holzenberger,
T. Peacock,
T. R. Akylas

要旨

The generation of internal gravity waves by a vertically oscillating cylinder that is tilted to the horizontal in a stratified Boussinesq fluid of constant buoyancy frequency N, is investigated. Simple kinematic considerations reveal that for a cylinder inclined by a given angle ϕ to the horizontal, there is a cut-off frequency, $N\sin\phi$, below which there is no longer a radiated wave field. This result is confirmed by supporting laboratory experiments.

1. 緒言

The 'St. Andrew's Cross' experiment performed by Mowbray & Rarity (1967) is one of the most celebrated studies of internal gravity waves. For this experiment, a cylinder aligned horizontally with a plane of constant gravitational potential is oscillated vertically with small amplitude in a density stratification of constant buoyancy frequency (which corresponds to top figure 1 with $\phi\to 0$ $(\chi\to\theta)$). The wave disturbance generated by the oscillating cylinder, instead of circular wave crests, features four wave beams that emanate from the cylinder (top figure 1b with $\chi\to\theta$), forming a cross pattern whose opening is determined by the dispersion relation.

Here, we step away from the canonical St. Andrew's Cross to consider a more generic setting that has not been previously explored, and in so-doing we find results that are profoundly different and potentially of broad interest. Specifically, we study internal wave generation by a vertically oscillating cylinder that is tilted with respect to the horizontal (figure 1) (Kataoka et al. 2017). This forcing arrangement leads to a variant of the classical St. Andrew's Cross that has features with no counterpart in the corresponding horizontal cylinder problem. For example, for a given tilt of the cylinder there is a cut-off frequency below which there is no longer a radiated wave field. Furthermore, three-dimensional effects due to the finite length of the cylinder, which are minor in the horizontal configuration, here become a significant factor and eventually

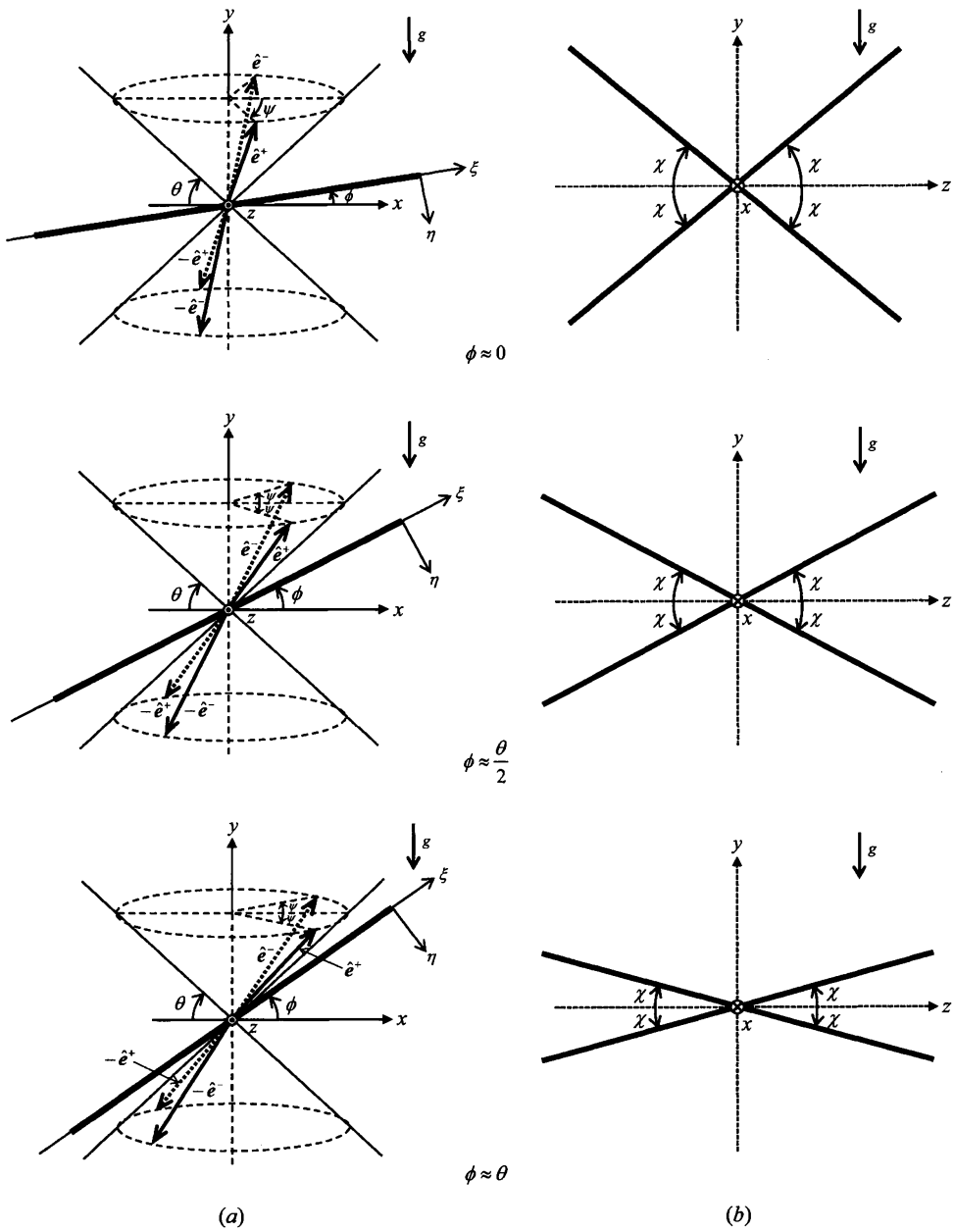

Fig. 1 Geometry of wave beams induced by infinitely long line forcing tilted to the horizontal by ϕ and oscillating with frequency $\omega = \sin\theta$: (*a*) three-dimensional view; four beams propagate in the directions $\pm\hat{e}^{\pm}$ and form an oblique cross; (*b*) intersection of the beams with the vertical *yz*-plane. Cases of three tilt angles ($\varphi \approx 0$, $\varphi \approx \theta/2$, $\varphi \approx \theta$) are shown.

dominate the wave field as the cut-off frequency is approached. These results follow from elementary linear wave theory and are also confirmed by supporting laboratory experiments.

2. 無限に長い傾斜棒からのビーム

We discuss the geometry of the steady-state internal wave pattern induced by time-harmonic line forcing, modelling an oscillating long thin cylinder, in an unbounded, non-rotating, uniformly stratified Boussinesq fluid. Here, the forcing is taken to be infinitely long. Our analysis makes use of the well-known dispersion relation of internal gravity waves,

$$\omega = \sin\theta, \tag{1}$$

where ω is the dimensionless wave frequency (scaled with the constant background buoyancy frequency N) and θ is the inclination angle of the wavevector to the vertical (y) axis pointing upwards. As illustrated in figure 1(a), the wave source stretches along the ξ-direction in the xy-plane and is tilted to the horizontal (x) axis by an angle $0<\phi<\pi/2$, with z being the transverse horizontal direction. Similar to the classical St. Andrew's Cross due to horizontal forcing ($\phi=0$), the dispersion relation (1) being independent of the wavevector magnitude is key to the kinematic argument used below for deducing the wave pattern due to a tilted line source.

From elementary linear wave theory, the steady-state response to a time-harmonic source comprises plane waves at the driving frequency. The location of corresponding beams relative to the source is determined by the group velocity $\boldsymbol{c}_g = \nabla_{\boldsymbol{k}}\omega$, which is at right angles to $\boldsymbol{k}$ and must point away from the source, in keeping with the radiation condition. Specifically, as shown in figure 1(a), two beams are found above the line source and propagate towards $y\to\infty$ along the corresponding group-velocity directions

$$\hat{\boldsymbol{e}}^{\pm} = \left(\cos\theta\cos\psi, \sin\theta, \pm\cos\theta\sin\psi\right), \tag{2}$$

where

$$\psi = \cos^{-1}\left(\cot\theta\tan\phi\right); \tag{3}$$

the other two beams are located below the line source and propagate towards $y\to-\infty$ in the opposite directions.

Overall, the generated wave pattern is in the form of a cross that leans in the direction of the

forcing. This 'oblique' cross undergoes dramatic transformation as the source tilt angle ϕ is varied in the range $0 \le \phi \le \theta$. As indicated in figure 1(*a*), a measure of the cross opening is the angle ψ in (3), which decreases monotonically with ϕ, from $\psi = \pi/2$ for $\phi = 0$ to $\psi = 0$ for $\phi = \theta$. As a result, the classical St. Andrew's Cross for horizontal forcing ($\phi = 0$) gradually closes as ϕ is increased and ultimately degenerates to a single standing beam along the forcing (ξ) direction in the limit $\phi \to \theta$.

A convenient way to visualize this transformation is by considering the intersection of the oblique-cross wave pattern with the (vertical) *yz*-plane. Seen in this plane, the four cross arms are inclined at

$$\chi = \tan^{-1}\sqrt{\tan^2\theta - \tan^2\phi} \qquad (4)$$

to the (horizontal) *z*-axis, and form a symmetric configuration centred at the origin (figure 1*b*). The angle χ attains the maximum $\chi = \theta$ for the classical St. Andrew's Cross ($\phi = 0$) which lies in the *yz*-plane. As ϕ is increased and the cross leans towards the forcing, χ monotonically decreases and eventually $\chi \to 0$ as $\phi \to \theta$.

3. 棒が有限長さであることの影響

We now turn to the effects of finite length of the line source. These end effects become progressively more significant with increasing source tilt angle ϕ, and understanding their role is crucial in interpreting the experimental observations in Section 4.

As in the case of infinitely long forcing, the steady-state response to a time-harmonic line source of finite length L is again made of plane waves with wavevectors inclined to the vertical by a fixed angle θ, determined by the driving frequency $\omega = \sin\theta$. Thus, treating the forcing ends as point sources, the plane waves emitted there propagate along vertical cones of angle θ from the horizontal, and contaminate the four wave beams that emanate from the interior of the forcing. Specifically, for tilted forcing as sketched in figure 2(*a*), the dominant end effects are expected to come from the upper cone due to the left end and the lower cone due to the right end, as these cones are closest to the main body of the forcing, where the wave beams are generated. To illustrate our approach, we now discuss how end effects modify the wave beam pattern in the vertical *yz*-plane across the middle of the forcing ($x = 0$). As argued above, the combined response (see figure 2*b*) consists of the four beams (solid lines) found earlier (figure

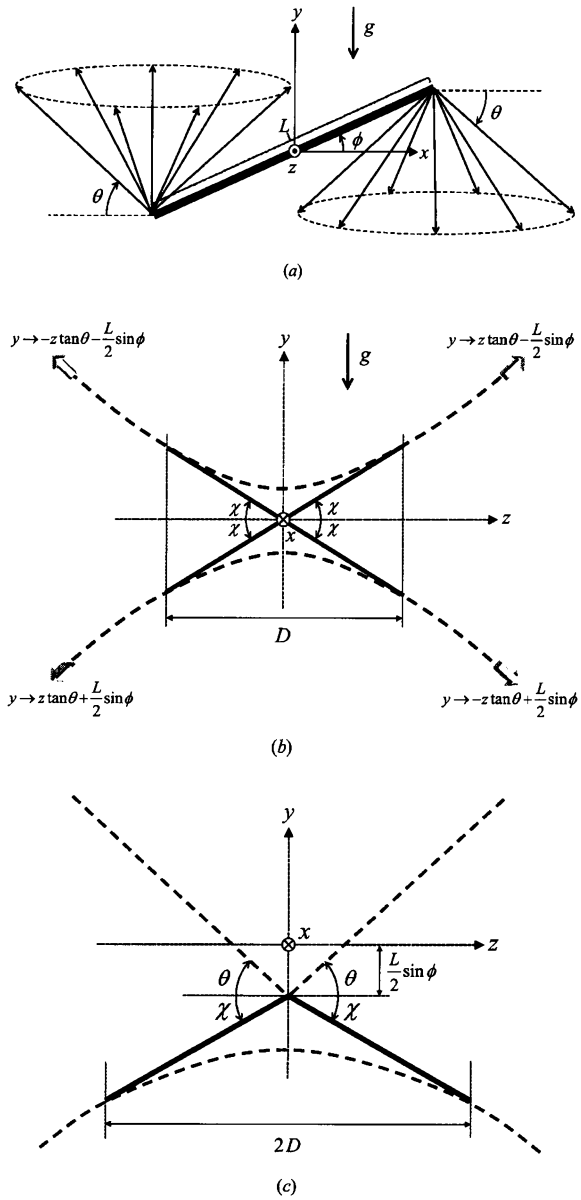

Fig. 2 Kinematics of internal waves generated by line forcing of finite length L, tilted at an angle φ to the horizontal and oscillating with angular frequency $\omega = \sin\theta$: (*a*) the dominant end effects arise due to plane waves that propagate along the two vertical cones shown; (*b*) intersection of the wave pattern with the vertical *yz*-plane across the middle of the forcing ($x = 0$); (c) intersection of the wave pattern with the vertical *yz*-plane across the lower end of the forcing ($x = -(L/2)\cos\varphi$). Here the dashed lines represent the end effects due to the two cones shown in (*a*), and the solid lines depict the four beams shown in figure 1(*b*), which emanate from the main body of the forcing.

1*b*) and the two hyperbolae (dashed lines) formed by the intersection of the *yz*-plane with the end cones shown in figure 2(*a*). From geometric considerations, it turns out that the four beam directions become tangent to these hyperbolae, and the wave beams remain distinct from the disturbances emanating from the ends, within a rectangle centred at the origin and of width

$$D = L\cos\varphi\sqrt{\frac{\tan^2\theta}{\tan^2\varphi}-1} \tag{5}$$

and height $D\tan\chi$ (figure 2*b*).

It should be noted that $D\to\infty$ when $\phi\to 0$ (horizontal forcing); in this instance, the wave beams coincide with the asymptotes of the two hyperbolae so the classical St. Andrew's Cross is hardly affected by the ends. As the tilt angle ϕ is increased and D is reduced according to (5), however, end effects are felt progressively more seriously. Finally, $D\to 0$ as the cut-off condition is approached ($\phi\to\theta$); in this limit, the forcing is tangent to the end cones in figure 2(*a*) so end disturbances totally interfere with the beams from the main body of the forcing. These kinematic results are confirmed by laboratory experiments in Section 4.

4. 実験結果

Our experimental study of the oblique-cross geometry focused on measuring the angle χ that the four cross arms make to the horizontal in the *yz*-plane (figure 2*b*). As discussed in Section 3, the response to tilted line forcing is always affected by the finite length of the source, and these end effects are amplified as the cut-off condition $\theta=\phi$ is approached. Specifically, in the *yz*-plane across the middle of the forcing (figure 2*b*), where the wave pattern is symmetric in y, the four wave beams due to the main body of the forcing remain intact within a rectangular region of width D given by (5), which shrinks to zero as $\theta\to\phi$. As a result, it becomes increasingly difficult to measure the angle χ when the driving frequency $\omega=\sin\theta$ of the cylinder approaches $\omega=\sin\phi$.

To tackle this issue, experimental data for χ was obtained in *yz*-planes closest to the cameras so as to observe the wave field near the lower end ($x=-(L/2)\cos\varphi$) of the cylinder. In this setup, as sketched in figure 2(*c*), the wave pattern is no longer symmetric as the wave beams emanating from the interior of the forcing appear only below the cylinder ($y<-(L/2)\sin\varphi$), in keeping with the beam propagation directions $-\hat{\boldsymbol{e}}^{\pm}$ relative to the

forcing (see figure 1*a*). Moreover, the disturbance above the cylinder ($y > -(L/2)\sin\varphi$) is entirely an end effect, from the intersection of the *yz*-plane with the end cone at the lower end of the cylinder (figure 2*a*), and turns out to be rather weak. As demonstrated below, this wave-field geometry makes it possible to accurately measure the beam angle χ even quite close to cut-off, by focusing on the wedge formed by the two beams just below the lower end of the cylinder.

Figure 3 shows snapshots of wave fields for $\phi = 44^\circ$ and $\theta = 49.5^\circ$ obtained in the *yz*-planes across the lower end of the cylinder ($L = 36\text{cm}$, diameter 2.5cm); top figure plotted the phase field of the vertical velocity component, which was chosen to maximize the clarity of the wave field structure. Consistent with the geometry in figure 2(*c*), the desired beam angle χ

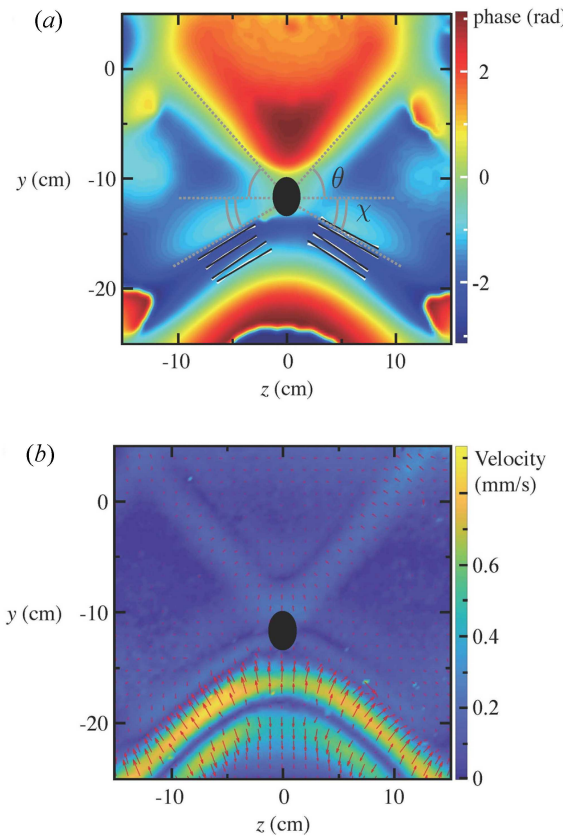

Fig. 3 (*a*) Phase field plot across the lower-end vertical plane of cylinder for $\varphi = 44^\circ$ and $\theta = 49.5^\circ$ ($\chi_{\text{theory}} = 33.6^\circ$ and $\chi_{\text{measured}} = 35.2^\circ \pm 1.1^\circ$). (*b*) Velocity amplitude plot (with superposed arrows) corresponding to phase results in (*a*). In each image, the black ellipse marks the location and area of the cylinder.

can be readily determined in the lower half of the field of view. The velocity amplitude plot (bottom figure 3) also shows good agreement with the kinematics presented in figure 2(*c*).

Experiments were run across a wide range of driving frequencies $\omega = \sin\theta$ for the three tilt angles $\phi = 0°$, $27°$ and $44°$, and the resulting data for χ as a function of $\theta = \sin^{-1}\omega$ is presented in figure 4, in which the error bars presented represent the standard deviation of the mean. There is generally excellent agreement between experiment and the theoretical predictions obtained from (4). Most notably, for fixed driving frequency ω, the beam projected angle χ is reduced as the cylinder tilt angle ϕ increases, and for non-zero ϕ there is a lower cut-off driving frequency corresponding to $\theta = \phi$ at which χ goes to zero; as expected, no radiated wave beams were observed below cut-off ($\theta < \varphi$).

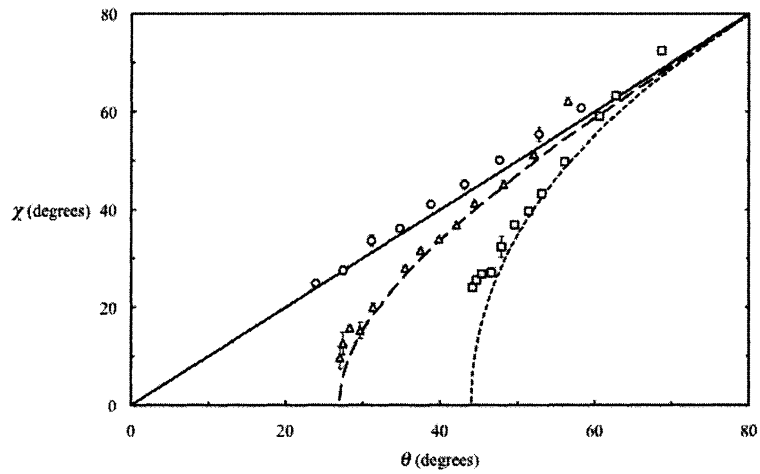

Fig. 4 Experimental data for the beam angle χ as a function of θ set by the driving frequency $\omega = \sin\theta$, for tilt angle $\varphi = 0°$ (circle), $\varphi = 27°$ (triangle) and $\varphi = 44°$ (square); the corresponding theoretical curves, obtained by (5), are included as solid, dashed and dotted lines, respectively. The error bars are the standard deviation of the mean.

参考文献

Mowbray, D. E. & Rarity, B. S. H., "A theoretical and experimental investigation of the phase configuration of internal waves of small amplitude in a density stratified liquid," *J. Fluid Mech.* **28** (1967) pp. 1–16.

Kataoka, T., Ghaemsaidi, S., Holzenberger, N., Peacock, T. & Akylas, T. R., "Tilting at wave beams: a new perspective on the St. Andrew's Cross," *J. Fluid Mech.* **830** (2017) pp. 660–680.